3D Surface Reconstruction from SEM/BSE multi-detector images

Vladislav A. Yastrebov

CNRS, Mines Paris - PSL, Centre des matériaux, Evry/Paris, France

August 2023 - Dec 2024

1. Overview

This script reconstructs 3D surfaces from SEM images obtained from at least 3 BSE detectors without prior knowledge of their orientation. The reconstruction is based on SVD decomposition, x and y gradient components are obtained using Radon transform, the full surface is reconstructed either by direct gradient integration or, preferably, by an FFT-based method by (Frankot et al., 1988). The whole strategy is based on the method described in (Neggers et al., 2021).

2. Method

Below we list the main steps of the method:

1. Load images $I_i, i \in [1, N]$ with $N \geq 3$ (see fig. 1)
   - It is supposed that the SEM image has information block (FOV, magnification, etc.) in the bottom side of the image. This block is automatically trimmed. If it is not the case, the user can manually trim the image.
   - Image names with the full path is stored in the log file.
   - If requested, a Gaussian filter is applied to the images.
2. A correlation matrix C_{ij} is constructed from the images I_i with components $C_{ij} = \sum_{x,y} I_i(x, y) I_j(x, y)$.
3. A Singular Value Decomposition (SVD) of the correlation matrix is performed: $C_{ij} = \sum_{k=1}^{N} U_{ik} S_k V_{jk}$.
4. The first three columns of the matrix U are used to construct the intensity image and two components of the gradient (along unknown principal directions) as follows (see fig. 2):

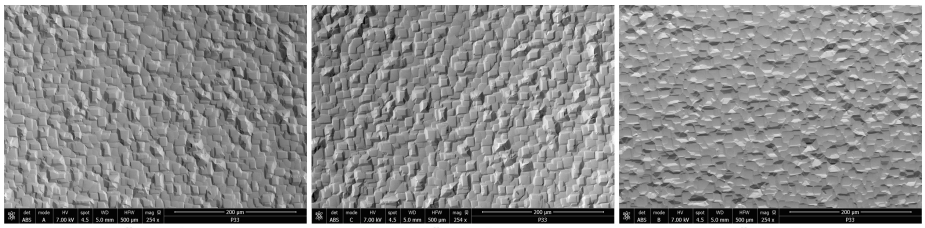

Figure 1: Original SEM images from three BSE detectors

- Intensity: $A = \sum_i U_{i1} I_i$.
- Gradient 1: $G_1 = \sum_i U_{i2} I_i / A$
- Gradient 2: $G_2 = \sum_i U_{i3} I_i / A$

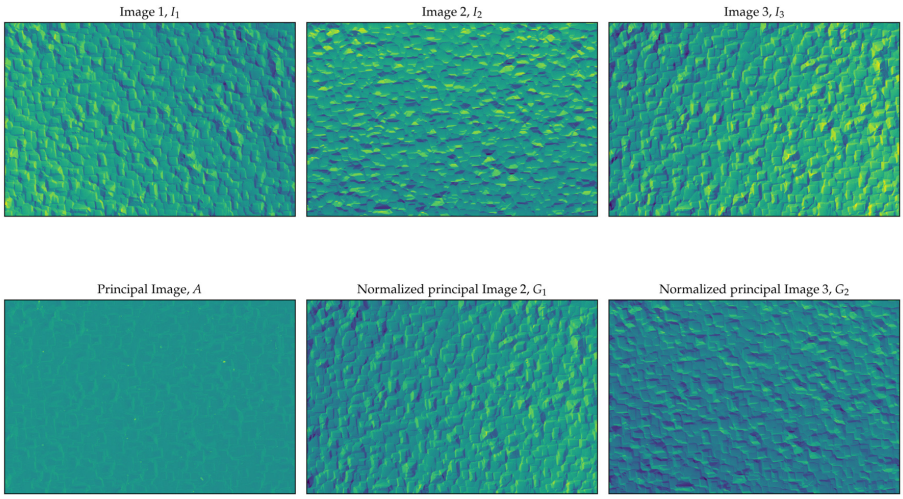

Figure 2: Original images I_1, I_2, I_3 obtained with three detectors and their principal components A, G_1, G_2 obtained through SVD

5. The x and y components of the gradient are obtained by using Radon transform of the gradient images G_1 and G_2. Specifically, we keep only the circular region of G_1 and null all data around (requirements of the Radon transfom module). Then we compute Radon transform $R(\theta)$ and compute its RMS for every value of θ (see fig. 3). Since Radon transform is computationally intensive, we apply it on G_1 only and discretize probe $\theta \in [0, \pi]$ in 180 points. The angle θ_1 corresponding to the minimum RMS is the angle of the first principal direction θ_1 (see fig. 3). The second principal

direction θ_2 is perpendicular to the first one. It could be evaluated in the same manner using G_2.

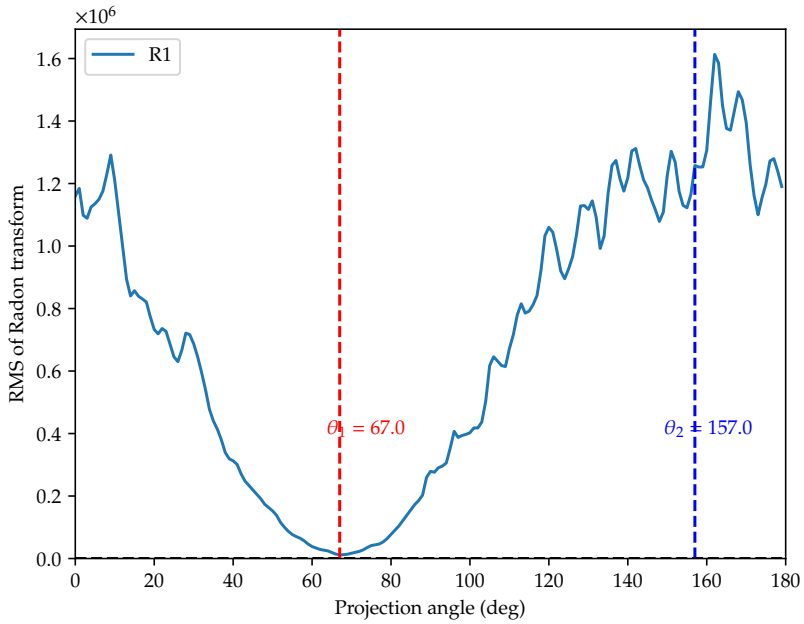

Figure 3: RMS of the Radon transform of the gradient image G_1

6. The x and y components of the gradient are then obtained as follows:
   - $G_x = G_1 \cos(\theta_1) + G_2 \cos(\theta_2)$
   - $G_y = G_1 \sin(\theta_1) + G_2 \sin(\theta_2)$

In addition, a macroscopic tilt is substracted from these gradients (see fig. 4). The tilt is computed as the average of the gradients over the whole image.

- $G_x = G_x - \langle G_x \rangle$
- $G_y = G_y - \langle G_y \rangle$

where $\langle G_x \rangle$ and $\langle G_y \rangle$ are the average values of the gradients G_x and G_y.

7. To reconstruct the surface from the gradients $G_x = \partial z/\partial x$ and $G_y = \partial z/\partial y$ we use alternatively two methods. The one is based on solving Poisson's equation in Fourier space, see (Frankot et al., 1988). The second method is a direct integration along x and y direction followed by minimizing distance between adjacent profiles and averaging between profiles integrated along x and y.

   1. The Frankot & Chellappa method, providing very high reconstruction

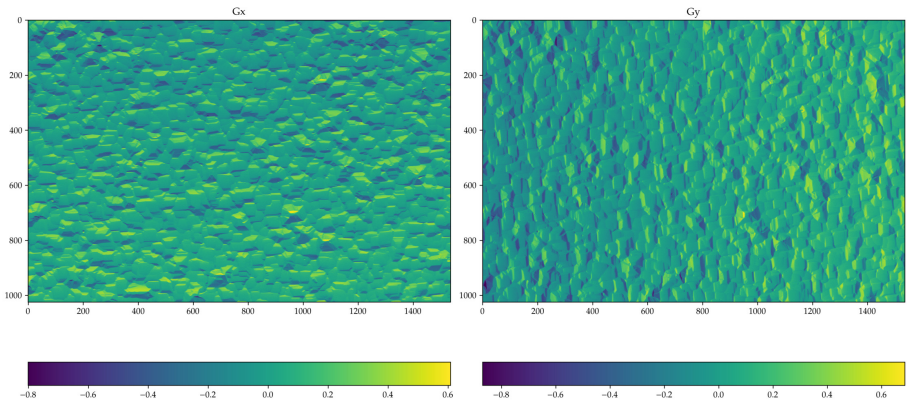

Figure 4: Gradients $G_x = \partial z/\partial x$ and $G_y = \partial z/\partial y$

quality (see fig. 5), is based on the following Fourier transform pair:

- $\partial^2 z/\partial x^2 \leftrightarrow -k_x^2 \hat{z}(k_x, k_y)$
- $\partial^2 z/\partial y^2 \leftrightarrow -k_y^2 \hat{z}(k_x, k_y)$

where $\hat{z}(k_x, k_y)$ is the Fourier transform of the surface $z(x, y)$ and k_x, k_y are the wave numbers. The surface is then reconstructed as follows:

- $\hat{z}(k_x, k_y) = -\frac{1}{k_x^2+k_y^2}\left(k_x \hat{G}_x(k_x, k_y) + k_y \hat{G}_y(k_x, k_y)\right)$
- $z(x, y) = \mathcal{F}^{-1}\left\{\hat{z}(k_x, k_y)\right\}$

where $\mathcal{F}^{-1}$ is the inverse Fourier transform and $\hat{G}_x(k_x, k_y)$ and $\hat{G}_y(k_x, k_y)$ are the Fourier transforms of the gradients G_x and G_y.

2. The method of direct integration, which in general provide results of much lower quality, is based on the following relations:

- Assume that the first profile along y is zero $z_x^{1,j} = 0$ for $j \in [1, N_y]$.
- Integrate the first profile along x direction $z_x^{i+1,1} = z_x^{i,1} + G_x^{i,1}\Delta x$ for $i \in [1, N_x - 1]$, where Δx is the pixel size.
- Integrate next profile along x direction $\tilde{z}_x^{i+1,j} = z_x^{i,j} + G_x^{i,j}\Delta x$ for $i \in [1, N_x - 1]$ and $j \in [2, N_y]$ and remove the average difference with respect to the previous provile $z_x^{i+1,j} = \tilde{z}_x^{i+1,j} - \langle \tilde{z}_x^{i+1,j} - z_x^{i+1,j-1} \rangle$.
- Repeat the previous step for all profiles along y direction using G_y to get $z_y^{i,j}$.
- Remove the average value of $z_x^{i,j}$ and $z_y^{i,j}$, i.e. $z_x^{i,j} = z_x^{i,j} - \langle z_x^{i,j} \rangle$ and $z_y^{i,j} = z_y^{i,j} - \langle z_y^{i,j} \rangle$.
- Construct the final surface as $z(x, y) = \frac{1}{2}\left(z_x^{i,j} + z_y^{i,j}\right)$.

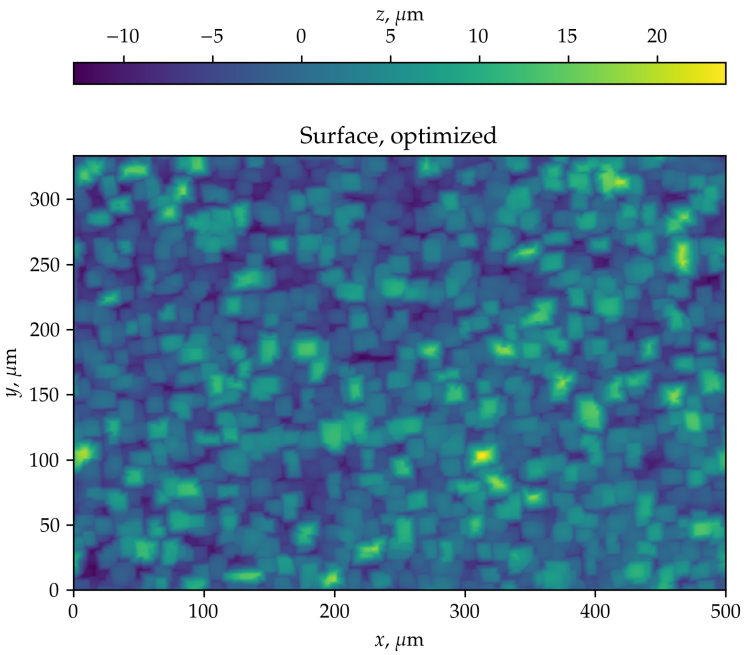

Figure 5: FFT reconstruction of the surface $z(x, y)$

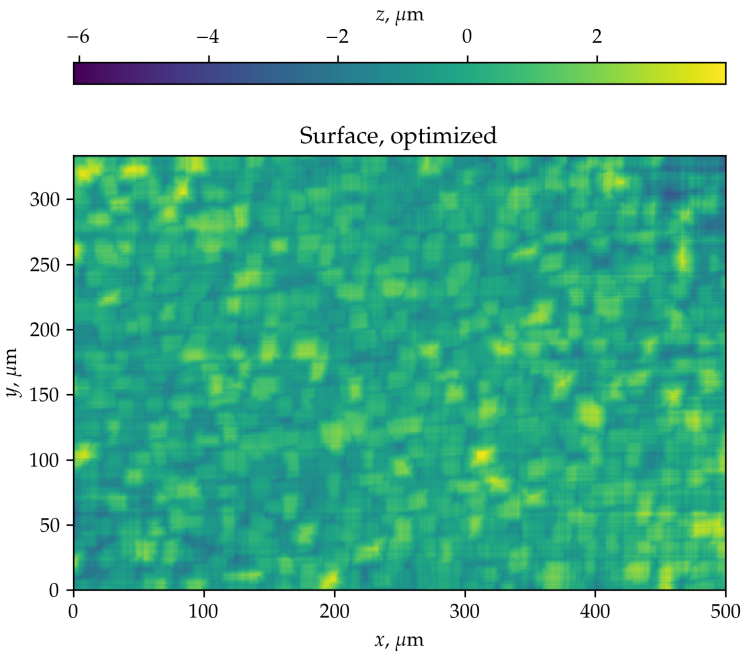

Figure 6: Reconstructed surface $z(x, y)$ using direct integration

8. The final step is the removal of the curvature of the surface. This is done by fitting a parabolic surface in principal axes

$$z(x, y) = \frac{x^2}{R_x^2} + \frac{y^2}{R_y^2} + z_0$$

and substracting it from the surface. The curvatures R_x, R_y and the off-set z_0 are obtained by the least square fitting procedure.

References

Frankot, R. T. and Chellappa, R., A Method for Enforcing Integrability in Shape from Shading Algorithms, *IEEE Transactions on Pattern Analysis and Machine Intelligence*, vol. **10**, no. 4, pp. 439–51, 1988.

Neggers, J., Héripré, E., Bonnet, M., Boivin, D., Tanguy, A., Hallais, S., Gaslain, F., Rouesne, E. and Roux, S., Principal Image Decomposition for Multi-Detector Backscatter Electron Topography Reconstruction, *Ultramicroscopy*, vol. **227**, p. 113200, 2021.